

This work was written as part of one of the author's official duties as an Employee of the United States Government and is therefore a work of the United States Government. In accordance with 17 U.S.C. 105, no copyright protection is available for such works under U.S. Law.

Public Domain Mark 1.0

<https://creativecommons.org/publicdomain/mark/1.0/>

Access to this work was provided by the University of Maryland, Baltimore County (UMBC) ScholarWorks@UMBC digital repository on the Maryland Shared Open Access (MD-SOAR) platform.

Please provide feedback

Please support the ScholarWorks@UMBC repository by emailing scholarworks-group@umbc.edu and telling us what having access to this work means to you and why it's important to you. Thank you.



In-Situ and Remotely-Sensed Observations of Biomass Burning Aerosols at Doi Ang Khang, Thailand during 7-SEAS/BASELInE 2015

Andrew M. Sayer^{1,2*}, N. Christina Hsu², Ta-Chih Hsiao³, Peter Pantina^{2,4}, Ferret Kuo⁵, Chang-Feng Ou-Yang⁵, Brent N. Holben², Serm Janjai⁶, Somporn Chantara⁷, Sheng-Hsiang Wang⁵, Adrian M. Loftus^{2,8}, Neng-Huei Lin⁵, Si-Chee Tsay²

¹ GESTAR/USRA, Columbia, Maryland, USA

² NASA Goddard Space Flight Center, Greenbelt, Maryland, USA

³ Graduate Institute of Environmental Engineering, National Central University, Chung-Li 32001, Taiwan

⁴ Science Systems and Applications, Inc, Lanham, Maryland, USA

⁵ Department of Atmospheric Sciences, National Central University, Chung-Li 32001, Taiwan

⁶ Silpakorn University, Nakorn Pathom, Thailand

⁷ Faculty of Science, Chiang Mai University, Chiang Mai, Thailand

⁸ ESSIC, University of Maryland, College Park, Maryland, USA

ABSTRACT

The spring 2015 deployment of a suite of instrumentation at Doi Ang Khang (DAK) in northwestern Thailand enabled the characterization of air masses containing smoke aerosols from burning predominantly in Myanmar. Aerosol Robotic Network (AERONET) Sun photometer data were used to validate Moderate Resolution Imaging Spectroradiometer (MODIS) Collection 6 ‘Deep Blue’ aerosol optical depth (AOD) retrievals; MODIS Terra and Aqua provided results of similar quality, with correlation coefficients of 0.93–0.94 and similar agreement within expected uncertainties to global-average performance. Scattering and absorption measurements were used to compare surface and total column aerosol single scatter albedo (SSA); while the two were well-correlated, and showed consistent positive relationships with moisture (increasing SSA through the season as surface relative humidity and total columnar water vapor increased), in-situ surface-level SSA was nevertheless significantly lower by 0.12–0.17. This could be related to vertical heterogeneity and/or instrumental issues. DAK is at ~1,500 m above sea level in heterogeneous terrain, and the resulting strong diurnal variability in planetary boundary layer depth above the site leads to high temporal variability in both surface and column measurements, and acts as a controlling factor to the ratio between surface particulate matter (PM) levels and column AOD. In contrast, while some hygroscopic effects were observed relating to aerosol particle size and Ångström exponent, relative humidity variations appear to be less important for the PM:AOD ratio here.

Keywords: Biomass burning; Aerosol; Remote sensing; In situ; 7-SEAS BASELInE.

INTRODUCTION

As part of the Seven South-East Asian Studies (7-SEAS) project (Lin *et al.*, 2013; Reid *et al.*, 2013), the Biomass-burning Aerosols & Stratocumulus Environment: Lifecycles and Interactions Experiment (BASELInE, Tsay *et al.*, 2013; 2016) was intended to probe physicochemical processes, interactions, and feedbacks related to biomass burning aerosols and clouds during the spring burning season (February–April) in southeast Asia (SEA). The 2015 segment of BASELInE included the deployment of

instrumentation at a range of dedicated sites across the region, including a supersite at Doi Ang Khang (DAK), in northwestern Thailand (19.93°N, 99.05°E, ~1.5 km above sea level; Fig. 1). DAK is close to the border with Myanmar and ~125 km north of Chiang Mai city. It is situated on top of a mountain, surrounded by forests and some agricultural fields. The site was selected as being representative for near-source biomass burning sampling in the region, which arises primarily from forest and agricultural waste burning (e.g., Tipayarom and Oanh, 2007; Chang and Song, 2010; van der Werf *et al.*, 2010; Lin *et al.*, 2013; Tsay *et al.*, 2016).

Instrumentation deployed at DAK during BASELInE in 2015 enabled the characterization of air masses influenced by biomass burning, common in SEA at this time of year, and included a Sun photometer as part of the Aerosol Robotic Network (AERONET; Holben *et al.*, 1998) as well as the

* Corresponding author.

E-mail address: andrew.sayer@nasa.gov

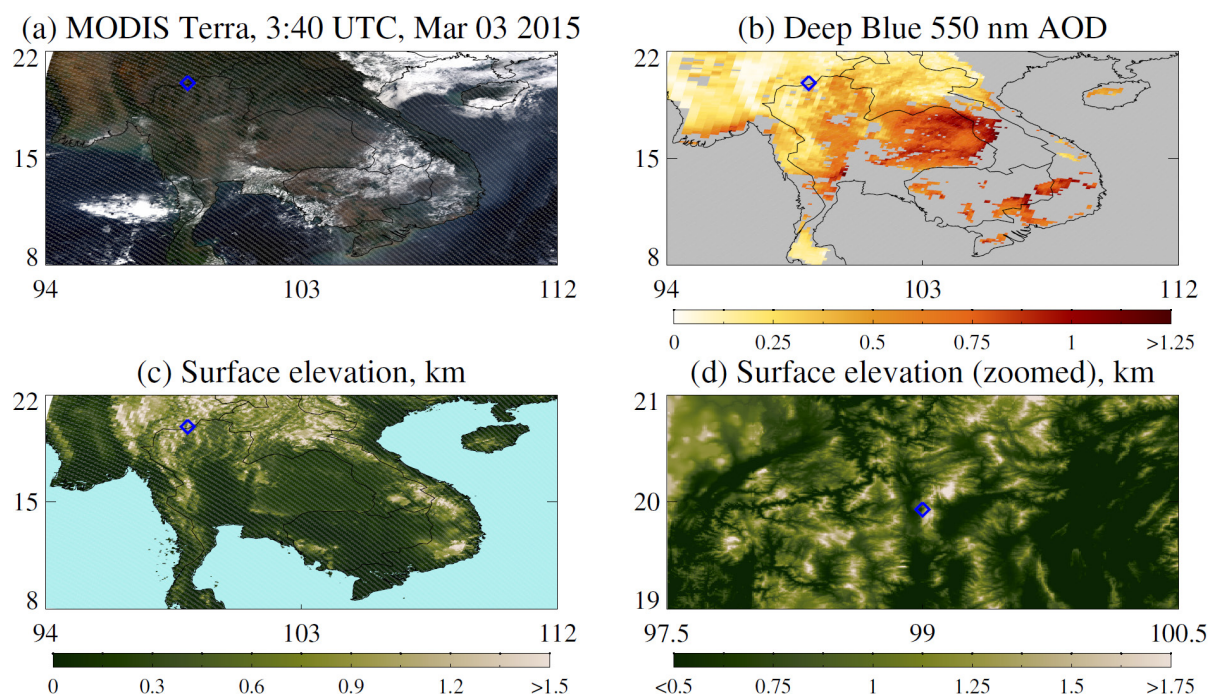


Fig. 1. (a) MODIS image from Mar 03 2015 showing DAK in the wider context of the study region. Panel (b) shows the MODIS Deep Blue AOD, (c) the surface elevation from MODIS and (d) zoomed-in near DAK from GTOPO30. In each panel, DAK is indicated by a blue diamond. In (b) pixels without AOD retrievals are indicated in grey, and in (c) pale blue areas indicate water.

Chemical, Optical, and Microphysical Measurements of In-situ Troposphere (COMMIT) mobile laboratory which is part of NASA's Surface-based Mobile Atmospheric Research & Testbed Laboratories (SMARTLabs, cf. <http://smartlabs.gsfc.nasa.gov>). This study presents first results from in-situ aerosol observations made by the COMMIT mobile laboratory at the 2015 DAK deployment, together with remotely-sensed (columnar) aerosol information from the AERONET Sun photometer and Moderate Resolution Imaging Spectroradiometer (MODIS) data products. It is intended to provide an overview of the data collected and a view towards the source regions contributing to smoke observed at DAK, as well as to study the relationship between these surface and columnar quantities.

DATA SETS AVAILABLE

In-Situ Aerosol and Trace Gas Measurements from SMARTLabs-COMMIT

Full details of the instrumentation active on the COMMIT mobile laboratory during the BASELInE deployment are provided by Pantina *et al.* (2016) and Tsay *et al.* (2016); a summary of data sets used herein is provided in Table 1. Briefly, available aerosol physical measurements included surface particulate matter (PM) mass loadings for particles with diameters smaller than 1, 2.5, and 10 μm (PM_{10} , $\text{PM}_{2.5}$, PM_{10} respectively). Spectral optical measurements included total surface extinction (PMEX) as well as sensors measuring scattering (NEPH) and absorption (PSAP and AETH) coefficients. The ambient surface-level relative humidity (RH) recorded on a weather station on-site through the

deployment had a median value of 40.3%, with the central 90% of the data within the range 23.2–79.7%, i.e., fairly low (see also discussion later). These mass and optical measurements were complemented by trace gas measurements of CO_2 , CO , O_3 , and SO_2 . Quality assurance procedures adopted by SMARTLabs standard operating procedure (SOP, cf. <http://smartlabs.gsfc.nasa.gov>) and applied to these data sets used in this analysis follow manufacturer guidelines and, for some instruments, additional correction factors. The instruments were operated continuously through the deployment, aside from maintenance periods.

Due to the high aerosol loading during some of the smoke events (particularly from March 10–21), the optical loss rate across the PMEX blue channel was from time to time larger than manufacturer recommendations, increasing the uncertainty on the data. This presents a challenge for the use of this instrument in aerosol-rich near-source environments. The green and red channels were not affected significantly by this limitation. However, hardware issues meant that the PMEX red channel was not active, aside from near the start of the deployment. As a result, PMEX data are not examined quantitatively in the present study.

Remotely-Sensed Aerosol Products from AERONET

AERONET data are available at several processing levels: Level 1.0 (raw), Level 1.5 (cloud-screened; Smirnov *et al.*, 2000), and Level 2.0 (cloud-screened and quality-assured). These include both direct-Sun data products (e.g., Holben *et al.*, 1998) such as columnar spectral aerosol optical depth (AOD), Ångström exponent (α), and columnar water vapor, and inversion products from almucantar scans

Table 1. Instrumentation deployed within the COMMIT mobile laboratory at DAK during BASELInE, together with sampling information and, where available, manufacturer-provided uncertainties (typically accuracy or precision).

Instrument	Measurement	Uncertainty	Temporal Resolution	Manufacturer
<i>Aerosols</i>				
Tapered Element Oscillating Microbalance (TEOM)	PM ₁	-	5 min	Thermo Fisher Scientific, USA
Beta Attenuation Monitor (BAM) 9600	PM _{2.5}	< 2.4 µg m ⁻³	1 hour	MetOne instruments, USA
BAM 10506	PM ₁₀	< 2.4 µg m ⁻³	1 hour	
Cavity Attenuated Phase Shift Extinction (PMEX)	Extinction at 445, 530, 630 nm	< 3.5 Mm ⁻¹	1 second	Aerodyne Research, Inc, USA
Nephelometer (NEPH) at ambient humidity	Scattering at 450, 550, 650 nm	-	5 min	TSI, Inc, USA
Aethelometer (AETH)	Absorption at 370, 470, 520, 590, 660, 880, 950 nm	5%	5 min	Magee Scientific, USA
Particle Soot/Absorption Photometer (PSAP)	Absorption at 470, 522, 550 nm	-	1 second	Radiance Research, Shoreline, USA (defunct)
<i>Trace gases</i>				
Dynamic gas calibrator	Calibration for gas monitors	-	1 min	Thermo Fisher Scientific, USA
CO ₂ analyzer	CO ₂	1%	1 min	Thermo Fisher Scientific, USA
CO analyzer	CO	0.1 ppm	1 min	Thermo Fisher Scientific, USA
SO ₂ analyzer	SO ₂	1% or 1 ppb	1 min	Thermo Fisher Scientific, USA
O ₃ analyzer	O ₃	1 ppb	1 min	Thermo Fisher Scientific, USA

(Dubovik and King, 2000) including aerosol particle size distribution, spectral complex refractive index, and single scattering albedo (SSA). Data are only raised from Level 1.5 to Level 2.0 after being returned for recalibration against AERONET master instruments and subjected to manual inspection; additional quality checks are performed on the inversion products (Holben *et al.*, 2006).

This study makes use of the Level 2.0 data products, which recently became available for the DAK deployment. For these Level 2.0 data, uncertainty on AERONET midvisible AOD is of order 0.01, and that of SSA (for AOD at 440 nm > 0.4, used here) ~0.03; additional uncertainty discussion is provided by Holben *et al.* (1998), Dubovik *et al.* (2000), and Sayer *et al.* (2014a). The majority of the results here use AERONET AOD interpolated spectrally to 550 nm; the spectral interpolation adds negligible uncertainty. Throughout this study references to AOD indicate the AOD at 550 nm, unless another wavelength is specified.

Remotely-Sensed Aerosol Products from MODIS

The most recent MODIS Collection 6 (C6) Deep Blue data set (Hsu *et al.*, 2013) provides spectral AOD and α over land; data for MODIS on both the Terra (10:30 am daytime local solar Equatorial crossing time) and Aqua (1:30 pm) have been validated and found to be temporally stable, with understood contextual biases (Sayer *et al.*, 2013, 2014b, 2015). This study uses the recommended Level 2

‘Best Estimate’ data set (Hsu *et al.*, 2013) which has a nominal pixel size of 10 km, averaged within a box of side 0.5° centered on DAK.

AEROSOL VARIATIONS DURING 7-SEAS/ BASELINE

Temporal Variation of Aerosol Properties

A time series of daily-averaged AERONET and MODIS columnar aerosol properties at DAK during BASELInE is shown in Fig. 2. The aerosol loading through most of February was low to moderate (0.2–0.5); a stronger event was observed around the start of March from day of year (DOY) 59–62, followed by a more prolonged burning period from around DOY 65–82. Following a data gap (due to cloudiness) the AOD was again low, aside from another event in early April (DOY 95–100). During the burning events, the temporal variability of AOD was often large, and could vary by > 1 in a single day. Values of α in the range 1.2–2 from AERONET, and ~1.8 in MODIS (corresponding to the maximum value allowed by the Deep Blue aerosol model), are consistent with a smoke-dominated aerosol column. Note that AERONET α is defined over the wavelength range 440–675 nm, while Deep Blue over these vegetated surfaces is defined over the range 470–650 nm, although this spectral mismatch is expected to lead to only minor discrepancy between the two.

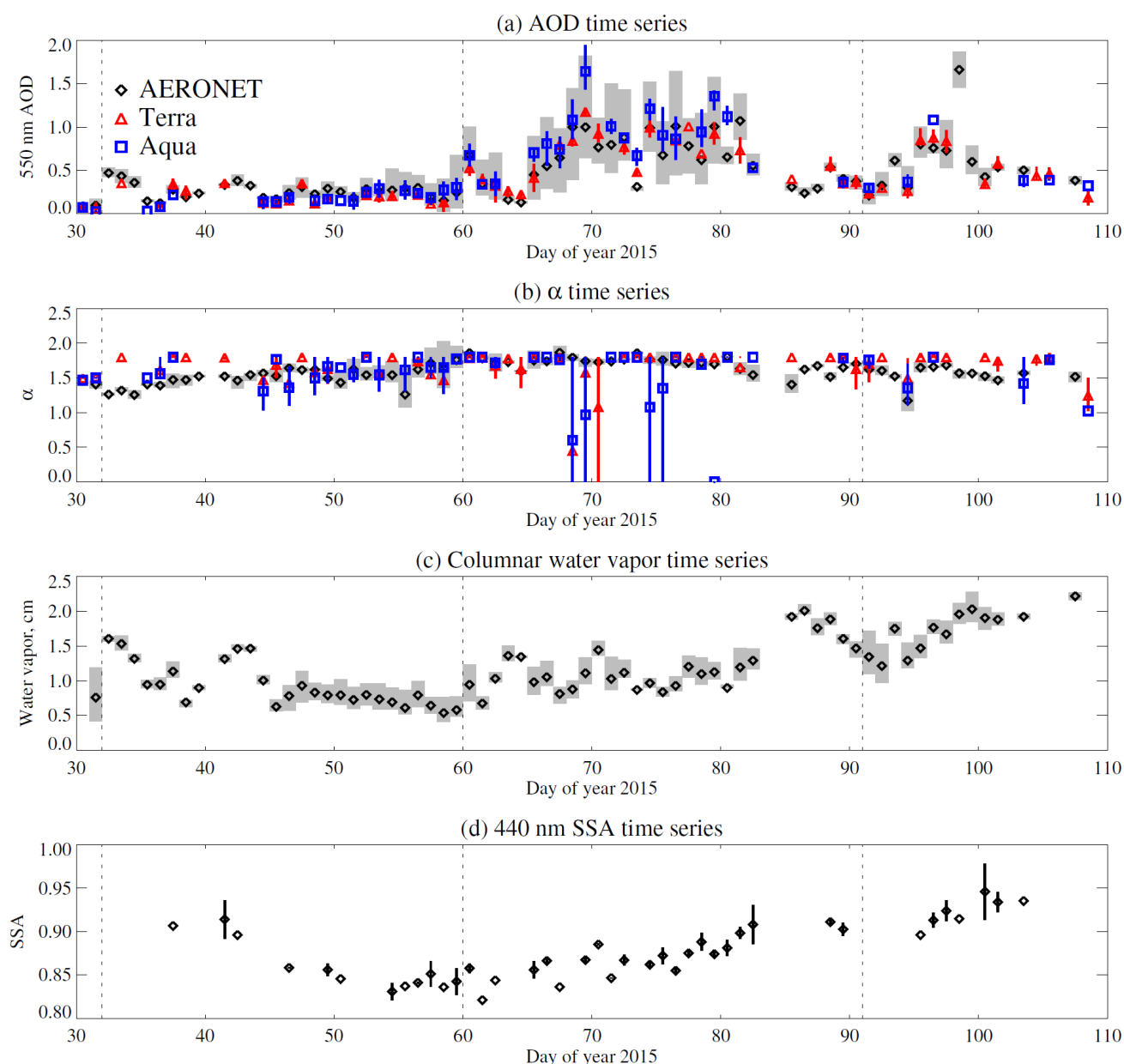


Fig. 2. Time series of AERONET and MODIS aerosol products: (a) AOD at 550 nm; (b) α ; (c) water vapor (AERONET only); and (d) SSA at 440 nm (AERONET only). For AERONET data in panels (a–c) symbols indicate daily mean and shaded grey the central 68% of the data. For SSA symbols indicate daily mean and standard deviation, due to limited sampling. For MODIS data symbols indicate mean and spatial standard deviation. Dashed vertical lines indicate the starts of February, March, and April.

The heterogeneous terrain and variability in aerosol loading and properties present a challenge for remote sensing of aerosol optical properties from space, thus it is useful to compare the Deep Blue retrievals to AERONET in this difficult environment. Fig. 3 presents a validation of the Deep Blue AOD against the AERONET data at DAK during this deployment; summary statistics are given in Table 2. The comparison protocol is as for other Deep Blue validation analyses (Sayer *et al.*, 2013, 2014b, 2015), namely MODIS data are averaged within 25 km of DAK and AERONET data within ± 30 minutes of the satellite overpass. The level of agreement is similar to global average

performance as established in the aforementioned studies. AOD tends to be higher at the times of the Aqua overpass (explored in more detail later) and thus quantities such as RMS error or bias are not directly comparable between the two, as retrieval uncertainties are functions of AOD. The retrieval uncertainty relative to AERONET is often expressed as $0.05 + 20\%$, for which both sensors are compliant $\sim 70\%$ of the time here (compared to a target of one standard deviation of the data, i.e., $\sim 68\%$). The C6 products also contain a pixel-level AOD uncertainty estimate which depends on AOD and geometry, known as ‘expected error’ (EE), defined relative to retrieved MODIS AOD, and for typical cases approximately

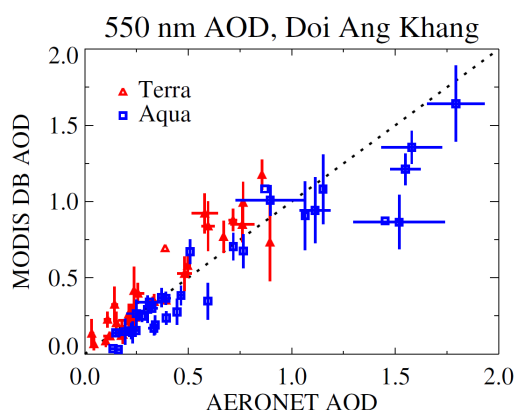


Fig. 3. Scatter plot of collocated AERONET and Deep Blue AOD at 550 nm data at DAK during BASELInE. Horizontal and vertical error bars indicate the standard deviations on AERONET and MODIS AOD, respectively, for those comparison points where more than one AERONET observation or MODIS retrieval was available.

Table 2. Statistics of AERONET/MODIS comparison at DAK during BASELInE, for the two MODIS sensors.

Satellite	Number of points	Correlation, R	RMS error	Median bias	Fraction within 0.05 + 20%	Fraction within EE
Terra	34	0.93	0.14	0.04	0.71	0.76
Aqua	33	0.94	0.20	−0.09	0.70	0.64

0.03 + 20% for Aqua (Sayer *et al.*, 2013) and 0.03 + 23% for Terra (Sayer *et al.*, 2015). Terra data show a higher fraction of compliance than Aqua, although with a small data volume it is important not to read too heavily into the statistics. The main point is that this comparison suggests that Deep Blue performance at DAK is consistent with the validation results of this data set elsewhere in the world. This is despite the high temporal variability of AOD (e.g., large AERONET variability bars in Fig. 3), and the high spatial heterogeneity of surface elevation (standard deviation ~350 m within the averaging box), which means that the MODIS retrievals may see a somewhat different vertical aerosol column than AERONET, dependent on the precise locations of MODIS pixels relative to the DAK site.

Returning to Fig. 2, both columnar water vapor and 440 nm SSA show an increasing tendency through the campaign, from ~0.5–2.5 cm and ~0.85–0.95 respectively; the correlation between daily mean columnar water vapor and SSA is significantly positive (ranging from 0.91 at 440 nm to 0.79 at 1020 nm). The SSA changes may be caused by fires from different fuel sources contributing to a changing smoke composition through the period, and/or increased humidification of the aerosol column later in the spring. Other studies (e.g., Eck *et al.*, 2013; Sayer *et al.*, 2014) have documented intra-seasonal dependence of smoke SSA in AERONET data. Fig. 4 shows Hybrid Single Particle Lagrangian Integrated Trajectory Model (HYSPPLIT) 48-hour back-trajectories (Draxler and Hess, 1998), computed using Global Data Assimilation System (GDAS) meteorological fields, for air masses ending at DAK's location and elevation, for select days drawn from this period. Throughout the deployment air masses arrived predominantly from Myanmar to the west, although as it uses coarse reanalysis fields HYSPPLIT cannot resolve the relative contributions of

transported and more local sources to the air mass at DAK. Most of these air masses had been vertically located up to around 2.5 km above sea level. The exception is the low-AOD period around DOY 85, at which time the air mass had arrived from the East (Thailand and Laos).

Fig. 5 shows MODIS monthly total fire counts (Giglio *et al.*, 2003) and mean daytime cloud fraction (Ackerman *et al.*, 1998; Baum *et al.*, 2012) from Terra. Spatial patterns from Aqua (not shown) are similar, although fire counts were higher in March in Aqua than Terra. These composites are consistent with Figs. 2 and 4 in that March exhibited more burning in Myanmar than the other months. The fairly low cloud cover over Myanmar/DAK, especially in February and March (< 37.5%), suggests that the apparent seasonality of fire counts over Myanmar should not be influenced strongly by cloud cover, and indeed the observability issues plaguing sampling of both satellite and ground-based aerosol monitoring systems (Chew *et al.*, 2011; Reid *et al.*, 2013) may be lessened compared to other parts of SEA. The median SSA varies from 0.87 at 440 nm to 0.81 at 1020 nm; this is more absorbing than smoke from Mukdahan in eastern Thailand (Sayer *et al.*, 2014a), which samples smoke from burning in Thailand and Laos, and so these differences may reflect the different source regions.

An analogue to Fig. 2, showing COMMIT observations during the active phase of its deployment (March to mid-April; shorter than the AERONET record), is shown in Fig. 6. The peaks identified in the columnar aerosol data (Fig. 2) are also seen in the ground-based data at the same times, confirming that the smoke plumes are sampled on the ground at DAK. The surface-level relative humidity (not shown) varied generally in the range 20–40% from the start of the deployment until DOY 81 (March 22); from then until DOY 89, which coincides with the period of decreased

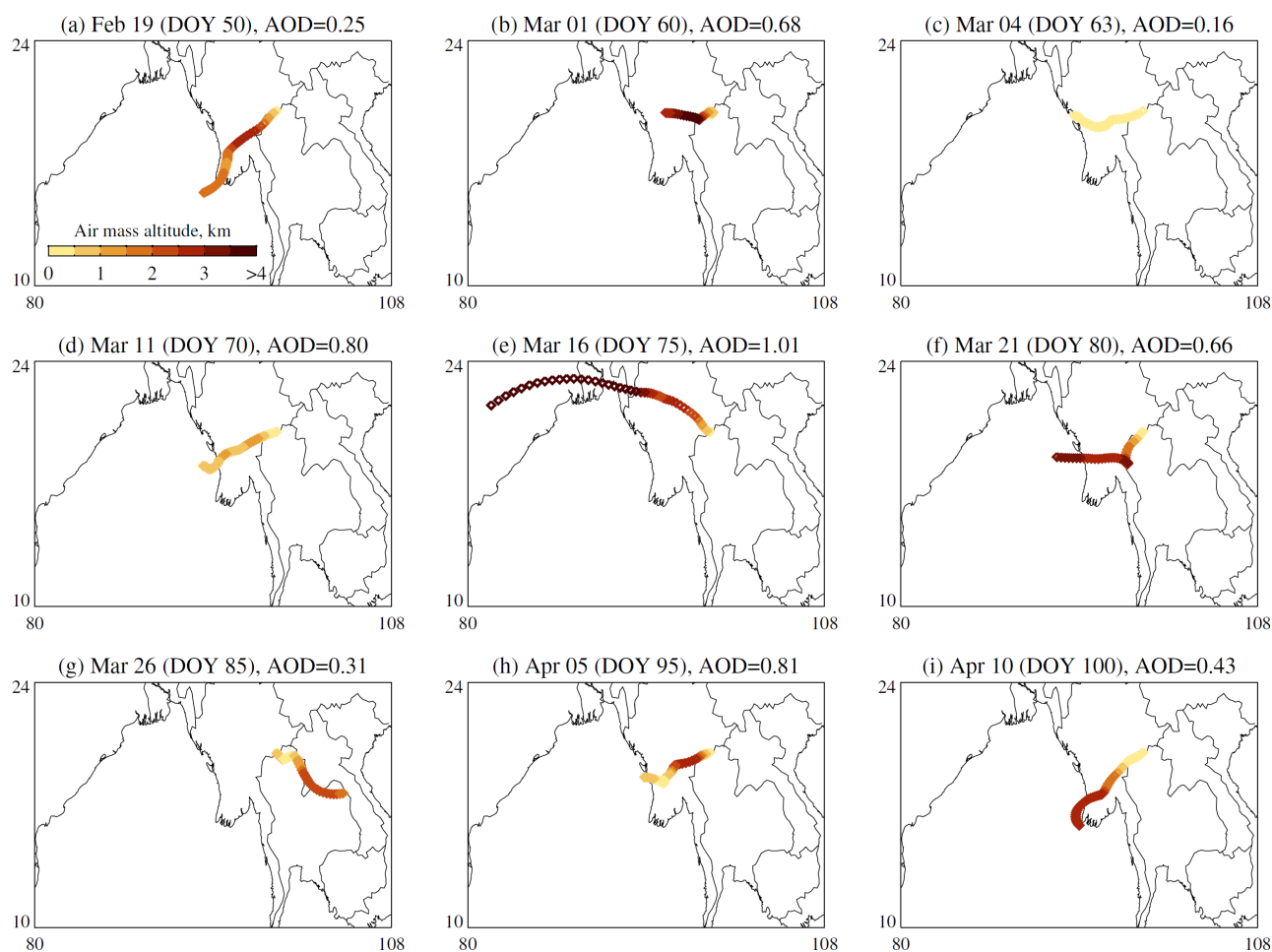


Fig. 4. HYSPLIT back trajectories, and air mass altitudes above ground level, for air masses arriving at DAK at 12 UTC on selected dates throughout BASELINe. AOD in panel captions indicates the AERONET daily mean AOD at 550 nm. Data shown at intervals of one hour.

aerosol loading in all the satellite and in-situ data, RH varied between 40–90% (note the RH monitor deployed at DAK caps at 90%). Rainfall occurred on several occasions between DOY 83 and 89, explaining the removal of aerosol particles during this period. This system moved in from the south-east (e.g., Fig. 4). For the final part of the deployment (DOY 90, March 31 onwards) RH varied in the range 20–50%. Thus, for the bulk of the periods with high aerosol loading, RH was low ($< 45\%$). The diurnal ranges of RH and surface air temperature were typically around 20% and 8°C , respectively, and their cycles (as expected) anticorrelated. Temperature varied largely within the range $18\text{--}27^{\circ}\text{C}$, although was $\sim 5^{\circ}\text{C}$ cooler during the high-humidity period.

Fig. 7 presents a more detailed view of three days (DOY 77–79) during a strong smoke event, along with planetary boundary layer height (PBLH) above surface from the NASA Modern-Era Retrospective analysis for Research Applications (MERRA; Reinecker *et al.*, 2011), at $0.5^{\circ} \times 0.625^{\circ}$ horizontal and hourly temporal resolution, interpolated to the DAK location. The recently-released version 2 (‘MERRA2’) is used (see Bosilovich *et al.*, 2015 for information on this version). This illustrates that, aside from mid-morning to evening, DAK is near the top of or

above the planetary boundary layer. This explains the increase of AOD throughout the day, even in fairly short interval (three hours) between Terra and Aqua overpass times, and suggests that most of the smoke plumes extended to the surface. This is also consistent with temporal correlation in spikes in surface (i.e., PM, scattering, absorption, CO_2) and column (i.e., AOD) measurements.

A limitation of the MERRA data is that it is a reanalysis product in a region that is particularly heterogeneous, and thus may face additional issues of representativeness. The quality of the PBLH data is likely variable in space and time, and it has not been evaluated rigorously at present (A. da Silva, personal communication). This means that the MERRA PBLH should not be interpreted too quantitatively. However, the basic features of the PBLH in Fig. 7 are consistent with micropulse lidar (MPL) profiles collected during spring 2014 at DAK (Wang *et al.*, 2015), which showed a similar strong diurnal cycle of the aerosol layer linked to an expansion and contraction of the PBLH, which gives confidence that the basic structure is sensible. Wang *et al.* (2015) also observed occasional ‘detached’ aerosol layers, likely from longer-ranged transport. Unfortunately, while MPL measurements were also collected during the

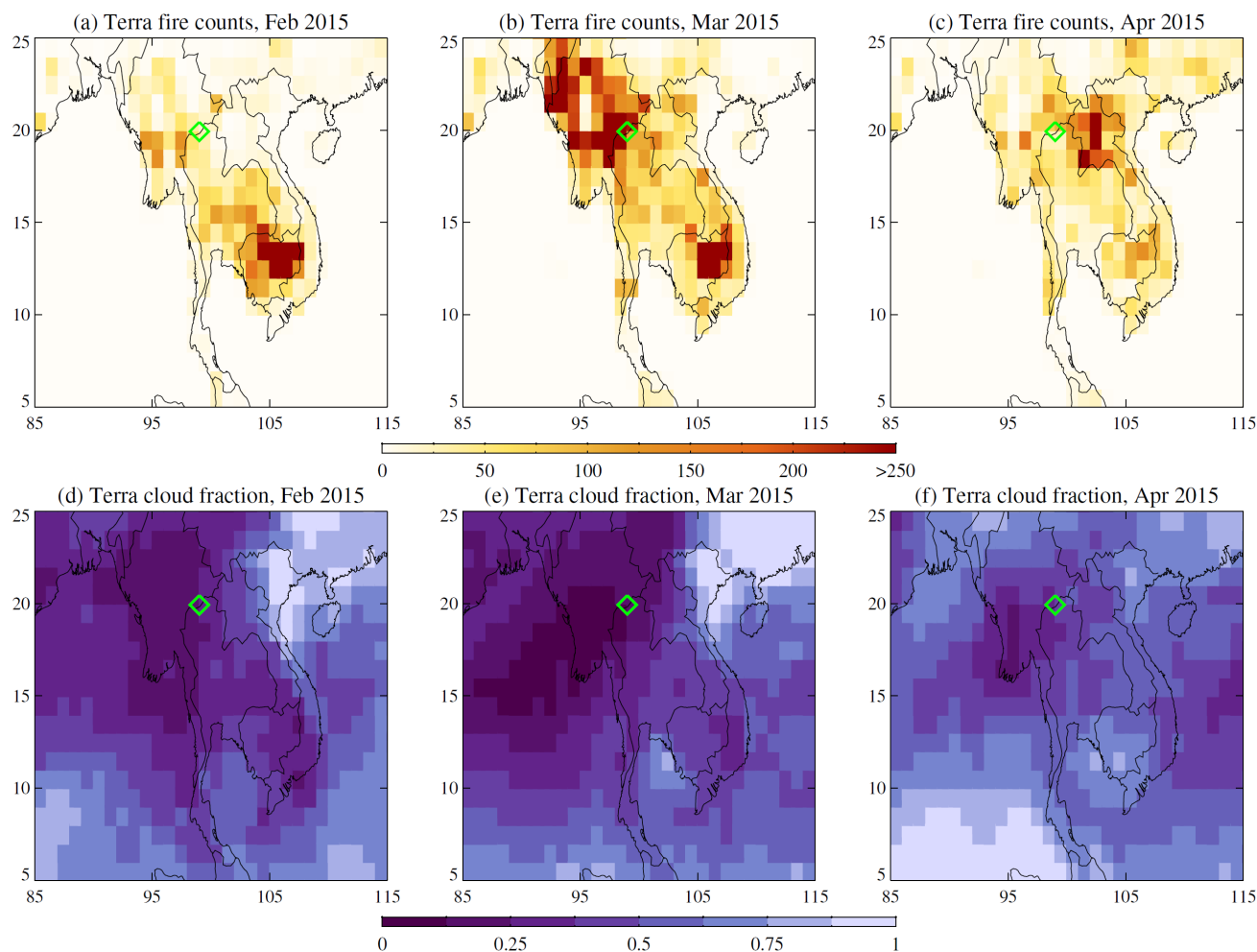


Fig. 5. MODIS fire counts (top row) and daytime cloud fraction (bottom row). DAK is indicated by a green diamond.

2015 deployment, these data are not yet available as they are awaiting processing and quality control (E. Welton, personal communication).

These data are also unable to answer questions about the relative contributions of more long-range transported smoke vs. local sources of smoke (or other aerosols) to the aerosol burden at DAK. For example, upslope/downslope transport of local aerosols to the site may affect the surface and total column data in different ways if they have different optical properties. Knowledge of the origin and age of the aerosol observed during particular periods would be useful to ascertain how variability in optical properties relates to factors such as source, ageing effects, and humidification. It is, unfortunately, difficult to answer these questions with the available data: the fairly coarse nature of e.g., MERRA and HYSPLIT is not adequate for these tasks. However it is important to be aware that regional-scale dynamics do not tell the whole story. Deployment of instrumentation for the optical/physicochemical properties and vertical distribution of aerosols at different elevations down the mountains, along with various points along the expected (i.e., from Myanmar, in this case) longer-range smoke transport pathways, would be helpful in this regard. As diurnal variability is so important in this region, the next generation of advanced

geostationary platforms, such as the recently-launched Himawari-8, will offer additional space-based constraints for these research topics, which have been largely unavailable from the current polar-orbiting satellite record.

Relating Surface and Columnar Single Scattering Albedo

The surface scattering (NEPH) and absorption (AETH, PSAP) measurements can be used to compute the at-surface aerosol SSA (as the scattering coefficient divided by the sum of scattering and absorption coefficients), to provide a comparison with the columnar SSA retrieved by AERONET. For this purpose the data were aggregated to hourly temporal resolution and NEPH, PSAP, and AETH scattering/absorption converted to match the AERONET SSA wavelengths of 440 and 675 nm using the Ångström power law. The source AETH and PSAP absorption coefficients are well-correlated ($R = 0.96$ – 0.97 , not shown); AETH absorption is slightly lower overall (median relative offset 22% for the blue band and $\sim 7.5\%$ for green and red bands), with the offsets becoming more pronounced at higher absorption strength ($> 200 \text{ Mm}^{-1}$). The agreement between SSA derived from the two becomes poorer because of this nonlinearity, and because the absorption represents a minority of the total extinction.

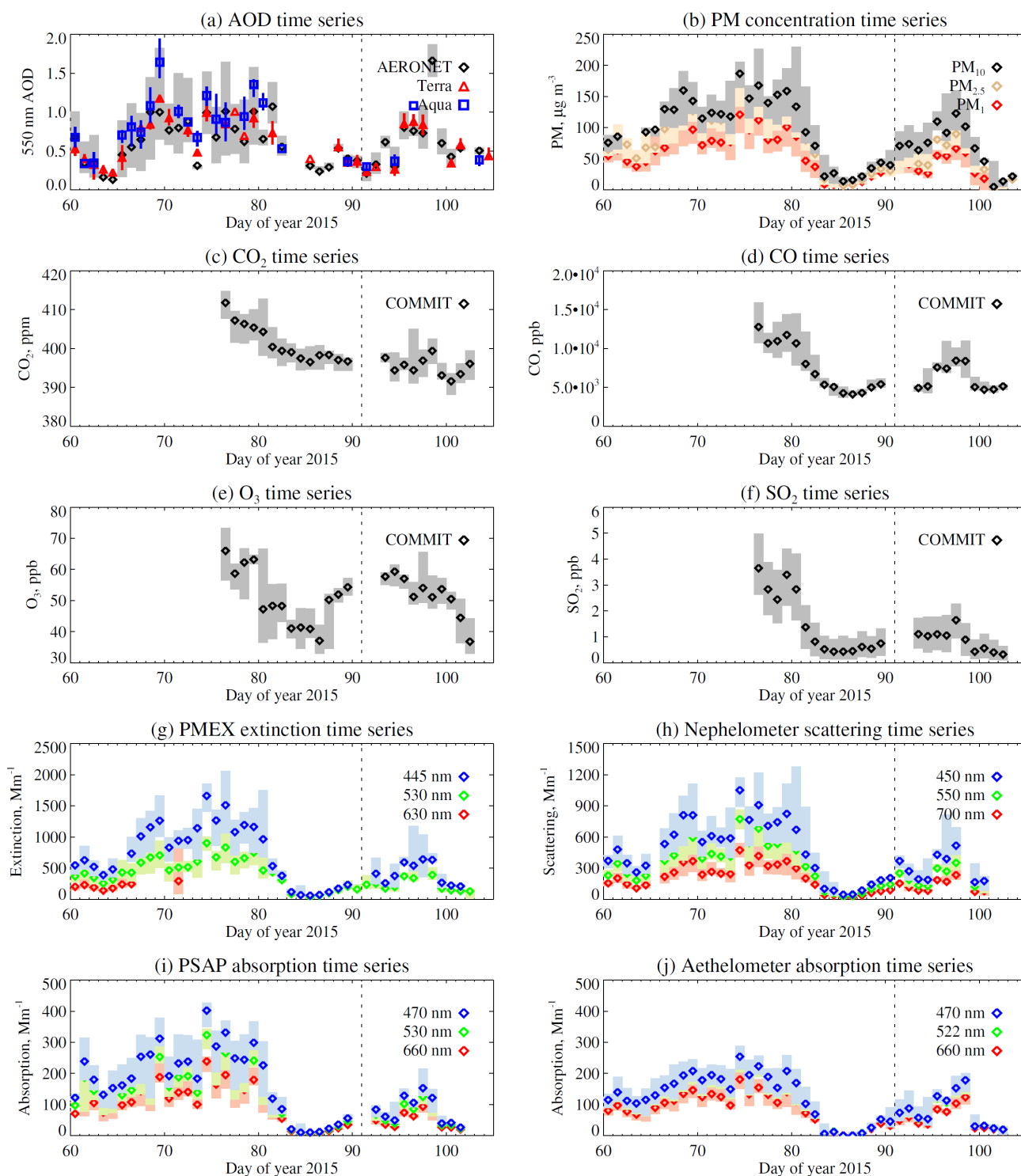


Fig. 6. As Fig. 2, except for aerosol and trace gas measurements taken by SMARTLabs-COMMIT during its deployment at DAK; AERONET /MODIS AOD data are shown for context.

The results of this comparison are shown in Fig. 8. In all cases the ground-based SSA is lower than the columnar SSA, although the two are positively correlated. Correlations are stronger for the NEPH + PSAP combination (0.79 at 440 nm, 0.88 at 675 nm) than NEPH + AETH (0.65 and 0.72 respectively). The SSA differences (median biases -0.12 to -0.17) are several times larger than the nominal AERONET

SSA uncertainty (~ 0.03 ; Dubovik *et al.*, 2000). Despite this, the SSA derived from AERONET and NEPH + PSAP exhibit a similar dynamic range (~ 0.15) across the deployment. This, and the strong correlation, suggests that the two are tracking real changes in the aerosol loading, and that the NEPH + PSAP combination may be more reliable (even though it has a slightly more negative offset against AERONET), although

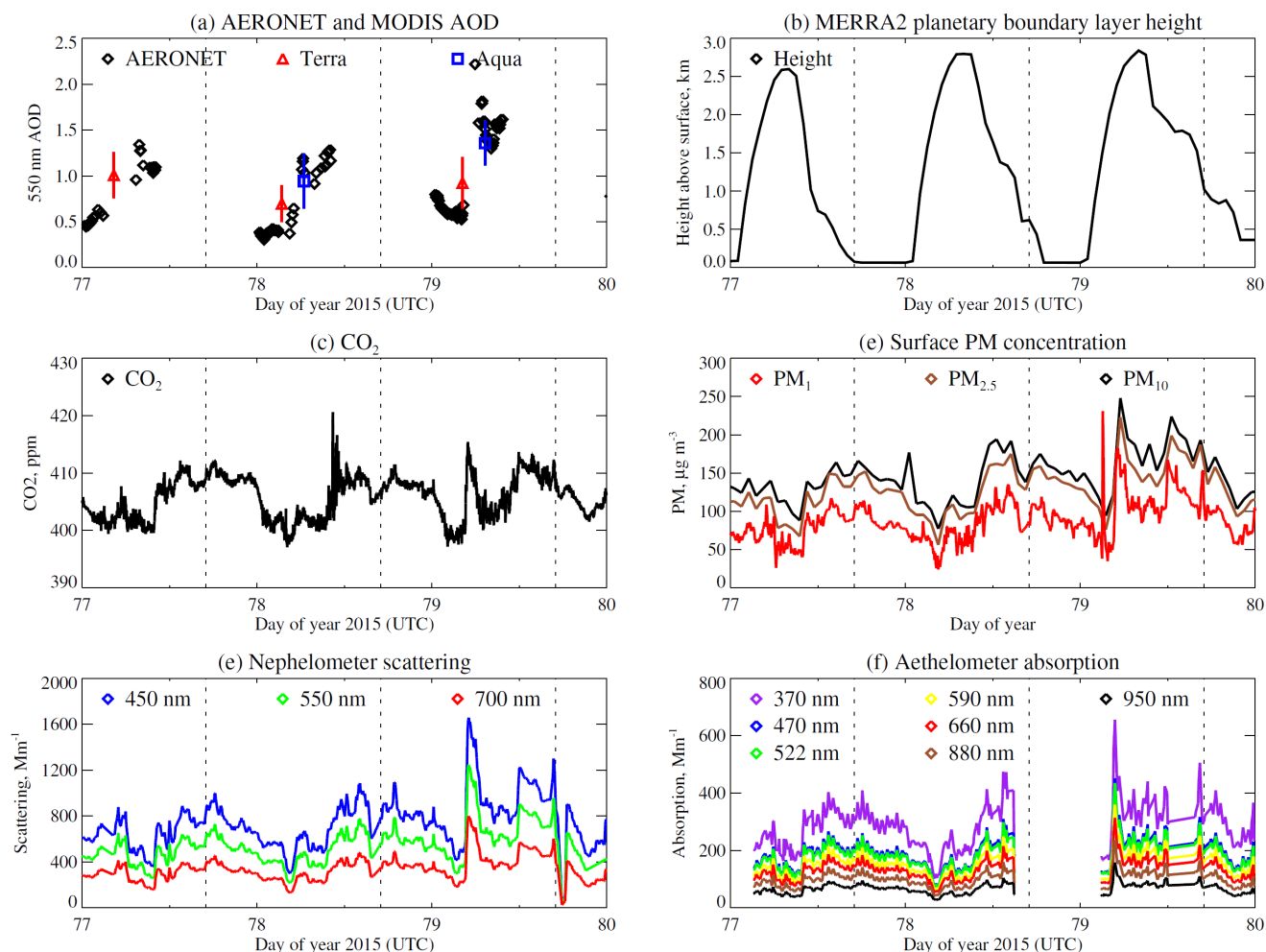


Fig. 7. Diurnal variability of surface and columnar smoke-related quantities during an intense smoke period, plus MERRA2 planetary boundary layer height. Note the time axis is defined in terms of UTC; vertical dashed lines indicate midnight local solar time.

again the data volume is small. Indeed, the COMMIT SOP includes large correction factors to AETH absorption (Arnott *et al.*, 2005), which reduce the absorption by up to ~50%, and it is possible that the corrections applied to this sensor in these conditions have a larger residual error than the PSAP measurements.

It is difficult to determine conclusively the contributions of different factors to the lower SSA in surface than column data. One explanation for the low offset could be that the NEPH scattering is underestimated, or PSAP/AETH absorption both overestimated. However to make the average SSA come into agreement, either NEPH scattering would have to increase by approximately a factor of two, or PSAP/AETH absorption would have to decrease by the same amount; instrumental artifacts of this magnitude seem unlikely. Another is sampling concerns: the in-situ observations sample smoke at ground level, whereas AERONET retrieves a column-effective SSA, so heterogeneities in smoke vertical properties, and/or the presence of weakly-absorbing aerosols in the column above the smoke layer, could also result in offsets.

The combination of instrumentation available allows the

feasibility of some of these hypotheses to be examined. The NEPH has a particle size cutoff of 2.5 μm diameter (AETH and PSAP do not) and so NEPH scattering will not include the contribution from any aerosol particles larger than this. However, the median AERONET fine-mode fraction of AOD (not shown) for the points included in these SSA comparisons is 0.98 at 440 nm and 0.96 at 675 nm, i.e., the NEPH size cutoff should have a negligible effect on total scattering for these cases, provided that the surface-level and column aerosol composition are the same. The median surface $\text{PM}_{2.5}/\text{PM}_{10}$ ratio is slightly lower (0.86 for the times coincident with NEPH + AETH points, 0.79 for AETH + PSAP points). This suggests that the fraction of coarse-mode aerosol may be larger at the surface than in the total column, but as aerosol extinction is more closely related to area than volume, the expected effect of this on extinction would be smaller than the 15–20% this mass ratio would imply. In any case, this could still not explain the approximate factor of two in either absorption or scattering needed to bring the data sets into agreement. The values of α (between 440 and 675 nm) from AERONET and surface measurements are also similar, with median values between 1.65 and 1.75

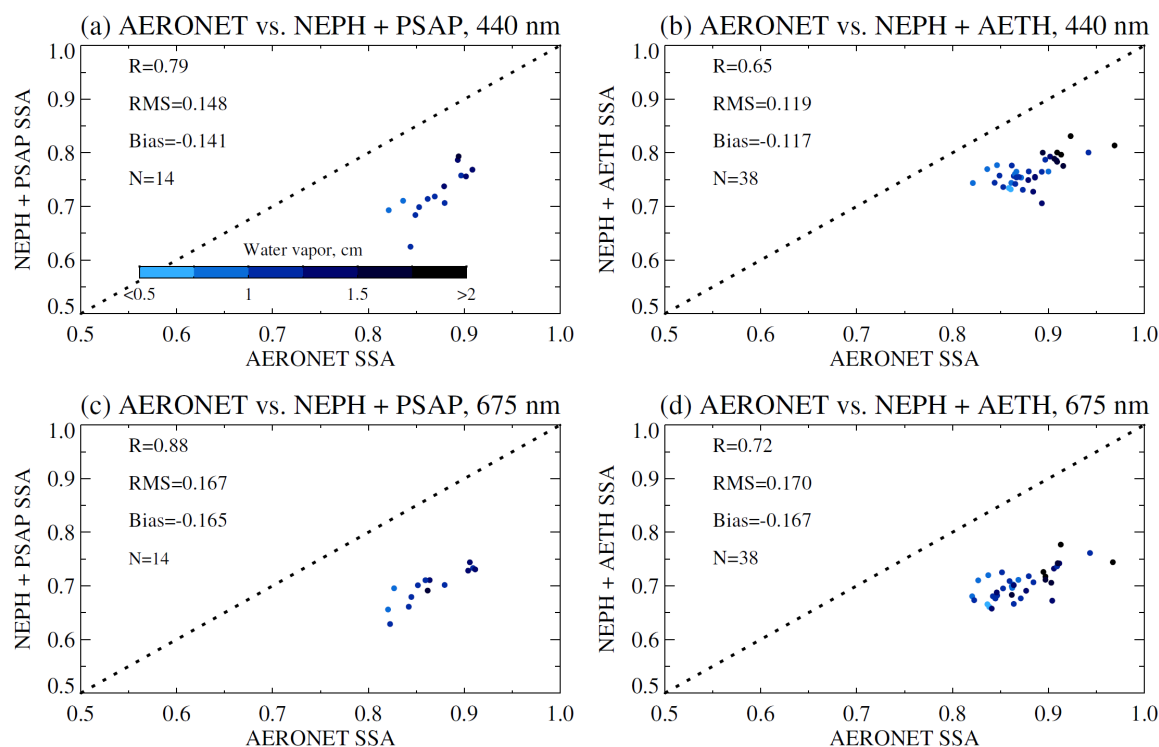


Fig. 8. Comparison between surface (NEPH+PSAP or AETH) and column (AERONET) SSA at (top) 440 nm and (bottom) 675 nm. Statistics include the correlation coefficient (R), root mean square (RMS) difference, median (in situ – AERONET) bias, and number of matchups (N). The color scale indicates the AERONET columnar water vapor for each data point.

for the collocated data, again indicating that the fine mode is optically dominant at both surface and total column.

The correlations (not shown) between daily-average AERONET SSA and water vapor in daily data are almost as strong in the hourly data ($R = 0.79$ and 0.70 at 440 and 675 nm). Similar albeit weaker correlations are found between in-situ surface SSA and surface RH measured at DAK ($R = 0.69$ and 0.68 for AETH, 0.65 and 0.49 for PSAP, at 440 and 675 nm respectively; note these correlations represent all available in situ SSA data, not the small subset where there is a temporal match with AERONET in Fig. 8), suggesting that some of the variability in both surface and column SSA is driven by variability in moisture, and that this is reflected in moisture within the smoke plume as well as the total column (i.e., the water and smoke are vertically collocated to an extent). Note that the RH for the times when AERONET and surface SSA are both available was fairly low (median 42.9% , and central 68% of the data from 32.7 – 63.8%). In comparison, AERONET AOD and SSA were essentially uncorrelated ($R = -0.08$ at 440 nm, 0.02 at 675 nm) suggesting no SSA-dependence of AOD.

Systematic biases in the AERONET SSA could also contribute to the offset, although biases of this magnitude seem unlikely to account for the majority of the difference. Validation of AERONET SSA is difficult but several studies have provided comparisons with estimates from different data sources. Using similar instrumentation to that available in this study (NEPH + PSAP), Leahy *et al.* (2007), Johnson *et al.* (2009), and Schafer *et al.* (2014) reported agreement

generally within AERONET uncertainties between AERONET column SSA and in-situ (airborne) measurements for cases of biomass burning, mixed dust and smoke, and North American urban/continental aerosols respectively. Chaudry *et al.* (2007) compared SSA for urban aerosols in Xianghe, China and found that, when AERONET and in-situ SSA differed, in-situ SSA was more absorbing and vertical inhomogeneities and local aerosol sources led to the difference (i.e., sampling reasons). Reid *et al.* (2005) discuss some of the difficulties with in-situ SSA characterization (largely related to quantification of absorption), and note that in-situ SSA estimates are often more absorbing than remotely-sensed (AERONET) ones. One other potential source of error in the AERONET inversions is the assumption that the refractive index is the same for all particle sizes; this can lead to errors if both modes have a strong optical presence (e.g., Xu *et al.*, 2015) as typically fine and coarse modes, with different chemical compositions, will have different refractive indices. However this should not be a factor for the cases presented here, due to the aforementioned strong optical dominance of the fine mode at both wavelengths examined.

In short, none of the individual likely candidates for disagreement between the two techniques can be identified conclusively as dominating the discrepancies observed. It therefore seems likely that some combination of instrumental issues and surface vs. columnar effects are important, although the high correlations between the data sets, and consistent relationships with water vapor/RH, are encouraging.

Column AOD as a Predictor for Surface PM

Due to the adverse effects of particulate matter on health (e.g., Pope, 2000), there has been considerable interest in recent years in using columnar AOD as a proxy for surface PM levels to allow for monitoring from space (e.g., review by Hoff and Christopher, 2009); as well as direct AOD-PM relationships, more sophisticated techniques involving meteorological factors have been developed and applied (e.g., van Donkelaar *et al.*, 2010, among others). Fig. 9 illustrates the AOD vs. PM relationship for the three different column AOD data sets, and three different PM size ranges, aggregated to hourly median values, and color-coded by MERRA PBLH. The PM/AOD ratio increases from PM_1 to $PM_{2.5}$ to PM_{10} as, although extra mass is being added, the additional coarser particles are less optically-active in the midvisible spectral region than the finer particles. Correlation coefficients range from 0.59 to 0.81, and show small variations between the three PM size ranges. Due to the small sample sizes these differences are not statistically significant, and neither are Terra/Aqua correlation differences. The AERONET data show the weakest correlations, as the slope of the AOD vs. PM relationship depends on the PBLH,

which shows large diurnal variability. A deeper boundary layer leads to a lower PM per unit AOD, and vice versa, which is intuitively expected if a given aerosol loading is dispersed throughout a deeper or shallower layer.

If the AOD data are normalized by PBLH (not shown), the correlation coefficients decrease by a factor of ~ 2 in the case of AERONET, and change insignificantly by ± 0.05 (either sign) for MODIS. In AERONET the outliers responsible for the decrease tend to be points where the PBLH is near zero, and so it is likely that this decrease in correspondence between the data sets is driven by limitations in the MERRA representation of PBLH in this highly heterogeneous terrain (cf. scale elevation gradients in Fig. 1 compared to the MERRA2 $0.5^\circ \times 0.625^\circ$ grid size). For MODIS these PBLH representation issues may be less severe because, with a near-constant overpass time, PBLH variations from day to day are small, so the effect of dividing by PBLH is closer to a linear scaling. Essentially, the day-to-day variation in PBLH at a given local time is smaller than the diurnal variability (see also Fig. 7). This suggests that, in terrain like this, despite their larger retrieval uncertainties, satellite AOD data may be more useful for estimating PM than

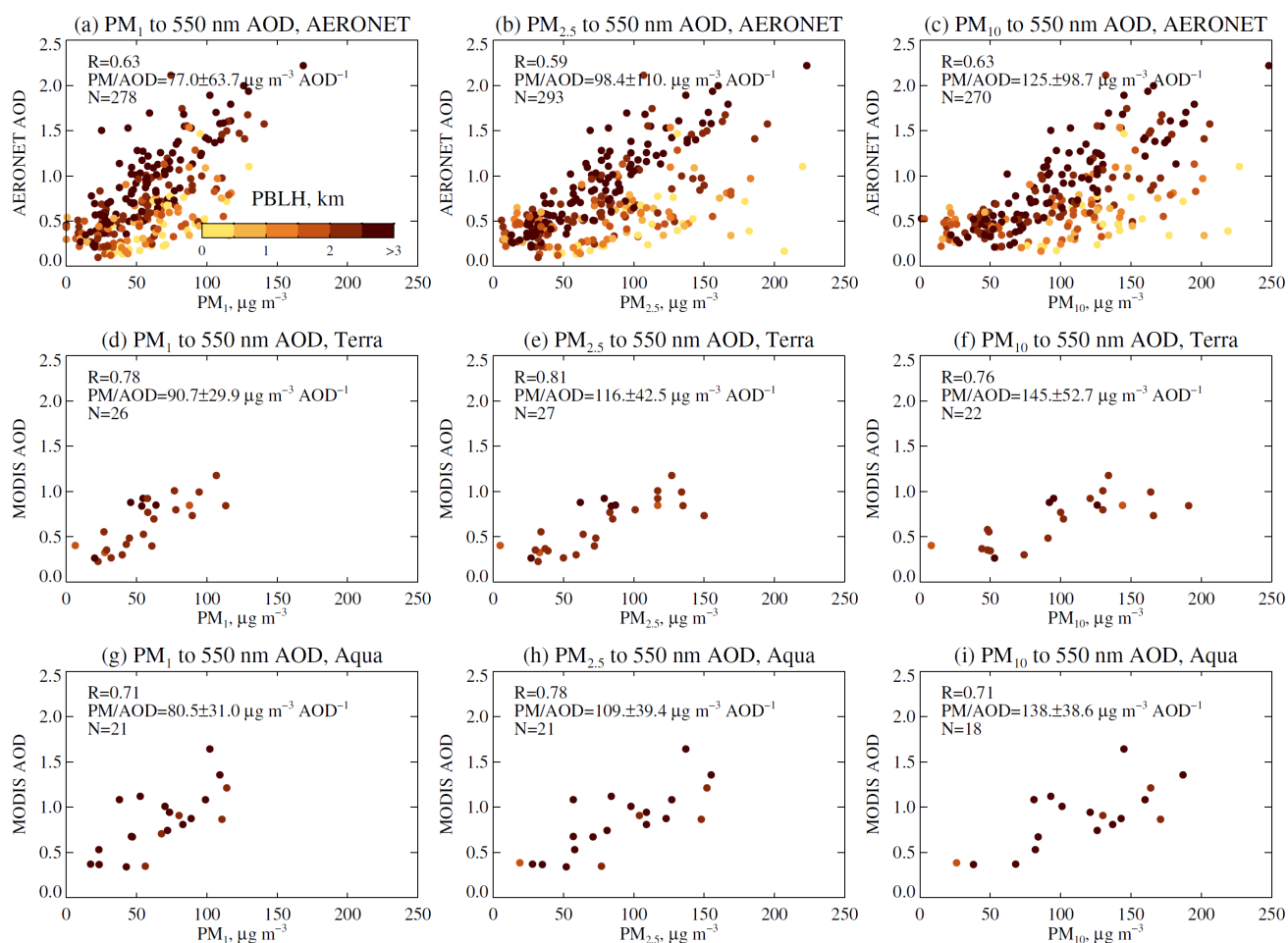


Fig. 9. Comparison between surface PM and column 550 nm AOD, for (top) AERONET, (middle) MODIS Terra, and (bottom) MODIS Aqua, and (left) PM_1 , (middle) $PM_{2.5}$, and (right) PM_{10} . Statistics include the correlation coefficient (R), median and standard deviation of the PM/AOD ratio, and number of matchups (N). The color scale indicates the MERRA2 PBLH above surface for each data point.

AERONET AOD, unless the AERONET AOD are restricted to a narrow time-of-day window, due to the near-constant overpass time of satellites minimizing variations in PBLH between observations. Note that vertical heterogeneity will also lead to scatter in the relationships. This can manifest through changes in PBLH (one factor leading to relative scatter in the PM/AOD ratio being larger for AERONET data), but additionally if a smoke plume is detached from the surface, as was observed from time to time in the 2014 deployment at DAK by Wang *et al.* (2015), then column AOD and surface PM would be uncorrelated.

Fig. 10 illustrates how the PM/AOD ratio (for AERONET) changes as a function of PBLH. The PBLH data are binned because, again, of uncertainties relating to MERRA's representation of the complex topography of this region. Each bin contains between 17 and 110 matchups of the hourly-aggregated data. The general tendencies discussed above—i.e., a decrease in PM/AOD as the PBLH deepens, or mass cutoff decreases—are apparent, as is the fairly large variability in this ratio, indicating the importance of secondary factors, and/or uncertainties in the AOD, PM, and MERRA data. Only AERONET AOD data are used for this figure due to their lower uncertainty, higher data volume, and better diurnal sampling than MODIS. The variability in the ratio also decreases as the PBLH increases. Although the available data volume is fairly small, one explanation for this could be that when the boundary layer is fairly deep the aerosol layer is fairly vertically-homogeneous, while it may be more heterogeneous (for example, with a relatively dense surface layer, which would increase PM/AOD, or an aerosol later detached from the ground, which would uncouple PM and AOD) when the boundary layer is shallow.

In contrast to PBLH, the PM/AOD ratio appears unrelated to either surface RH or total column water vapor (not shown). These two quantities are themselves either weakly or uncorrelated with PBLH ($R = 0.001$, 0.32 respectively) but fairly strongly ($R = 0.72$) correlated with each other. The weak but statistically significant correlation between PBLH and total column water vapor is, in the same way as the correlation between PBLH and AOD, consistent with the site's elevation and expansion of the boundary layer during the day. Despite these low correlations between moisture and

the PM/AOD ratio, compositing data across the deployment, there are statistically significant relationships between surface/columnar aerosol properties and RH (Fig. 11). Using linear least-squares regression, the AERONET-derived fine-mode effective radius (r_e) increases by $\sim 0.025 \mu\text{m}$ over the 20–60% RH range under which most of these data were collected. Note that the fairly high correlation and low estimated uncertainty on this relationship (Fig. 11(a)) result in part from the single outlier with RH of 90% (the maximum value recorded on the in situ data monitor) so this relationship should not be over-interpreted, although the statistics are similar if this data point is excluded. Both surface and columnar α (calculated from 440–675 nm) show a decrease over this RH range (Figs. 11(b)–11(d)), although the change is about twice the size in the AERONET data (-0.19) than surface data (-0.085 to -0.1). Lower α is also consistent with hygroscopic swelling of the fine mode aerosols. This AERONET/in situ difference may reflect increased aerosol hygroscopicity in the total column relative to the surface, although it seems more likely that instrumental uncertainties affect this since α is somewhat sensitive to spectral biases. These relationships are similar if AERONET column water vapor is used instead of surface RH (not shown). Some additional discussion of aerosol hygroscopicity during the deployment is provided by Pantina *et al.* (2016).

These results are consistent with smoke aerosols from many different burning sources being only weakly hygroscopic (e.g., Reid *et al.*, 2005 for a review of smoke optical properties), as well as the fairly low humidity through most of the deployment (Fig. 11), meaning that the observed changes in aerosol size/optical properties with humidity are fairly small. In contrast, in this rugged terrain, the PBLH changes by a comparatively large amount, which results in PBLH being the main controlling factor for the PM/AOD ratio here as opposed to changes related to aerosol water uptake. However, if these aerosols were transported further to regions of higher RH than in the present study, or over a region of less vertical variability in terrain altitude or PBLH, or if they change in composition due to further ageing or mixing, then the changing moisture content could have a more significant effect on the aerosol optical properties and the PM/AOD ratio than observed at DAK.

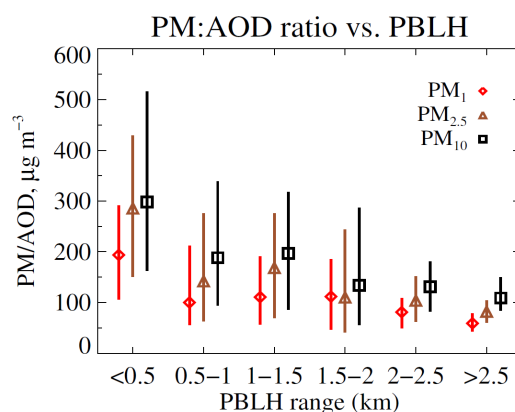


Fig. 10. Ratio of surface PM to AERONET AOD at 550 nm as a function of MERRA PBLH. Symbols indicate median values, and vertical lines the central 68% of the data, within each PBLH bin.

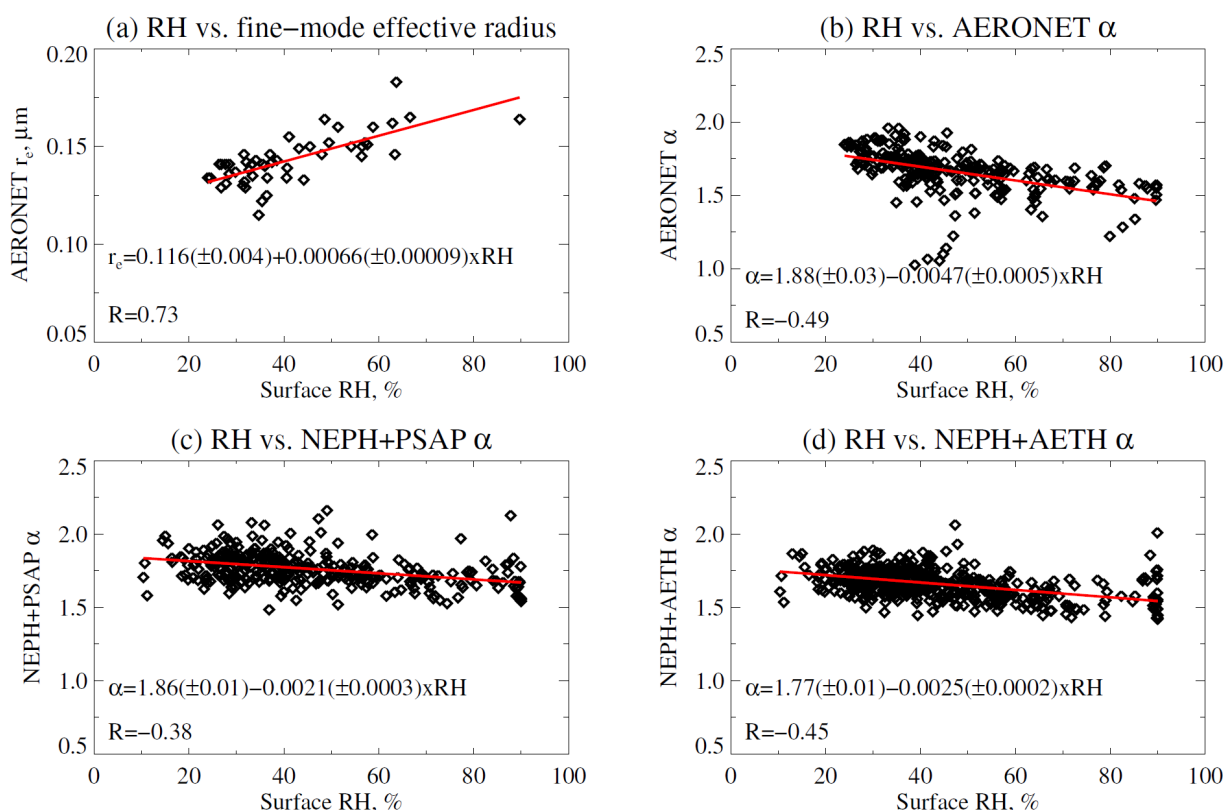


Fig. 11. Relationship between surface RH and (a) AERONET fine-mode aerosol effective radius, and α derived from (b) AERONET column, (c) NEPH+PSAP surface, or (d) NEPH + AETH surface data. The red lines show the linear least squares regression of the data, with regression equations (uncertainties indicate the one-standard-deviation confidence interval on coefficients) and correlation coefficients given in the panels.

CONCLUSIONS

The 7-SEAS/BASELInE experiment was intended to provide a multi-year ‘baseline’ characterization of biomass burning aerosols in SEA, taking a semi-Lagrangian perspective to examine chemical and optical properties near source and along the transport pathways. The location of DAK allowed for in-situ sampling of chemistry, mass and optical properties related to biomass-burning aerosols, predominantly from fires burning in Myanmar, during the spring 2015 deployment. This suite of instrumentation allowed analysis of this important part of the global aerosol cycle, from both a surface level and total column perspective, although important questions remain relating to, for example, the contributions of local vs. transported aerosol and how these vary diurnally.

AERONET Sun photometer validation of MODIS Deep Blue aerosol products revealed similar quality to global average performance, despite the complex terrain. AERONET also enabled a comparison of column-average SSA with surface measurements; although well-correlated, particularly for the combination of nephelometer scattering with PSAP absorption, there was nevertheless a low offset around 0.12–0.17 in the surface data. Based on previous comparisons of this type it is thought that the difference can be attributed to a combination of instrumental effects and vertical inhomogeneity of the aerosol column (more

strongly absorbing near the surface). Both showed consistent relationships of decreases in absorption (i.e. higher SSA) with increases in moisture, which occurred gradually from February to April.

A strong diurnal variation in observed aerosol loading, for both column and surface-level metrics, was linked to variability in planetary boundary layer depth. A corollary of this is that the column AOD vs. surface PM relationship exhibited less scatter using MODIS retrievals than AERONET direct-Sun observations, despite the high accuracy of the latter, because the relationship is dependent on the vertical structure of the aerosol field. However the practicality of applying the observed PM/AOD ratios outside of the DAK location in space is likely to be limited, because the same high spatiotemporal variability in aerosols resulting from the heterogeneous terrain is likely to mean that spatial patterns in AOD do not translate monotonically to spatial patterns in PM; this remains a limitation of remotely-sensed AOD as a PM proxy (e.g., Paciorek and Liu, 2009). Hygroscopic effects on aerosol size and optical properties were observed, but were comparatively unimportant for the PM/AOD ratio in this region and season.

7-SEAS/BASELInE contributes to the critically-needed database for these particle types, and enhances our knowledge of their influence on local and regional air quality, weather, and climate. This effort additionally facilitates concurrent studies of the potential impacts resulting from interactions

between these aerosols and cloud systems downwind of source regions (Tsay et al., 2013; Lee et al., 2014; Loftus et al., 2016; Tsay et al., 2016). The data collected throughout 7-SEAS is, for example, being used to constrain and evaluate modeling efforts aimed at better understanding aerosol lifecycles and their interactions with clouds from microphysical to regional scales. With knowledge of the ‘bigger picture’ of the aerosol life cycles gleaned from BASELInE, proposed future 7-SEAS experiments will co-locate measurement suites suitable for aerosol measurements and cloud profiling (e.g., the SMARTLabs COMMIT and ACHIEVE trailers) to focus on these interactions, which still face some challenges in understanding (Lin et al., 2014). The potential application of mature algorithms such as Deep Blue to next-generation geostationary satellite sensors, such as the recently-launched Advanced Himawari Imager on Himawari-8, and similar forthcoming sensors on other platforms, would improve the space-based constraints on some of these science questions by providing additional information on diurnal cycles in the region.

ACKNOWLEDGMENTS

This study was funded by the EOS program, managed by H. Maring. Further information about Deep Blue is available at <http://deepblue.gsfc.nasa.gov>. AERONET data are available from <http://aeronet.gsfc.nasa.gov>. MODIS atmospheric data are available from <http://ladsweb.nascom.nasa.gov>. The SMARTLabs website is <http://smartlabs.gsfc.nasa.gov>; data can be requested from PI S. C. Tsay. The authors gratefully acknowledge the NOAA Air Resources Laboratory (ARL) for the provision of the HYSPLIT transport and dispersion model (<http://www.ready.arl.noaa.gov>) used in this publication. GTOPO30 data are provided by USGS at <https://lta.cr.usgs.gov/GTOPO30>. L. Ellison is thanked for assistance obtaining the MODIS fire counts used in this study. The NASA Global Modeling and Assimilation Office and GES DISC are acknowledged for the creation and dissemination of MERRA2 (<http://gmao.gsfc.nasa.gov>), and A. da Silva and R. Govindaraju are thanked for assistance with, and discussions about, MERRA and MERRA2. The authors are grateful for the constructive comments of the two anonymous reviewers of this manuscript.

REFERENCES

- Ackerman, S.A., Strabala, K.I., Menzel, W.P., Frey, R.A., Moeller, C.C. and Gumley, L.E. (1998). Discriminating clear sky from clouds with MODIS. *J. Geophys. Res.* 103: 32141–32157.
- Arnott, W.P., Hamasha, K., Moosmüller, H., Sheridan, P.J. and Ogren, J.A. (2005). Towards aerosol light-absorption measurements with a 7-wavelength aethalometer: Evaluation with a photoacoustic instrument and 3-wavelength nephelometer. *Aerosol Sci. Technol.* 39: 17–29.
- Baum, B.A., Menzel, W.P., Frey, R.A., Tobin, D.C., Holz, R.E., Ackerman, S.A., Heidinger, A.K. and Yang, P. (2012). MODIS cloud-top property refinements for Collection 6. *J. Appl. Microbiol. Clim.* 51: 1145–1163.
- Bosilovich, M.G., Akella, S., Coy, L., Cullather, R., Draper, C., Gelaro, R., Kovach, R., Liu, Q., Molod, A., Norris, P., Wargan, K., Chao, W., Reichle, R., Takacs, L., Vikhliakov, Y., Bloom, S., Collopy, A., Firth, S., Labow, G., Partyka, G., Pawson, S., Reale, O., Schubert, S.D. and Suarez, M. (2015). MERRA-2: Initial Evaluation of the Climate. In *Technical Report Series on Global Modeling and Data Assimilation*, Koster, R.D. (Ed.), NASA/TM–2015-104606/Vol. 43, pp. 145.
- Chang, D. and Song, Y. (2010). Estimates of biomass burning emissions in tropical Asia based on satellite-derived data. *Atmos. Chem. Phys.* 10: 2335–2351.
- Chaudhry, Z., Martins, J.V., Li, Z., Tsay, S.C., Chen, H., Wang, P., Wen, T., Li, C. and Dickerson, R.R. (2007). In situ measurements of aerosol mass concentration and radiative properties in Xianghe, southeast of Beijing. *J. Geophys. Res.* 112: D23S90.
- Chew, B.N., Campbell, J.R., Reid, J.S., Giles, D.M., Welton, E.J., Salinas, S.V. and Liew, S.C. (2011). Tropical cirrus cloud contamination in sun photometer data. *Atmos. Environ.* 45: 6724–6731.
- Draxler, R.R. and Hess, G.D. (1998). An overview of the HYSPLIT_4 modeling system of trajectories, dispersion, and deposition. *Aust. Meteorol. Mag.* 47: 295–308.
- Dubovik, O. and King, M.D. (2000). A flexible inversion algorithm for retrieval of aerosol optical properties from Sun and sky radiance measurements. *J. Geophys. Res.* 105: 20673–20696.
- Dubovik, O., Smirnov, A., Holben, B.N., King, M.D., Kaufman, Y.J., Eck, T.F. and Slutsker, I. (2000). Accuracy assessments of aerosol optical properties retrieved from Aerosol Robotic Network (AERONET) Sun and sky radiance measurements. *J. Geophys. Res.* 105: 9791–9806.
- Eck, T.F., Holben, B.N., Reid, J.S., Mukelabai, M.M., Piketh, S.J., Torres, O., Jethva, H.T., Hyer, E.J., Ward, D.E., Dubovik, O., Sinyuk, A., Schafer, J.S., Giles, D.M., Sorokin, M., Smirnov, A. and Slutsker, I. (2013). A seasonal trend of single scattering albedo in southern African biomass-burning particles: Implications for satellite products and estimates of emissions for the world's largest biomass-burning source. *J. Geophys. Res.* 118: 6414–6432.
- Giglio, L., Descloitres, J., Justice, C.O. and Kaufman, Y. (2003). An enhanced contextual fire detection algorithm for MODIS. *Remote Sens. Environ.* 87: 273–282.
- Hoff, R.M. and Christopher, S.A. (2009). Remote sensing of particulate pollution from space: have we reached the promised land? *J. Air Waste Manage. Assoc.* 59: 645–75.
- Holben, B.N., Eck, T.F., Slutsker, I., Tanré, D., Buis, J.P., Setzer, A., Vermote, E., Reagan, J.A., Kaufman, Y.J., Nakajima, T., Lavenue, F., Jankowiak, I. and Smirnov, A. (1998). AERONET - A federated instrument network and data archive for aerosol characterization. *Remote Sens. Environ.* 66: 1–16.
- Holben, B.N., Eck, T.F., Slutsker, I., Smirnov, A., Sinyuk, A., Schafer, J., Giles, D. and Dubovik, O. (2006). AERONET's Version 2.0 Quality Assurance Criteria.

- Proc. SPIE* 64080Q.
- Hsu, N.C., Jeong, M.J., Bettenhausen, C., Sayer, A.M., Hansell, R., Seftor, C.S., Huang, J. and Tsay, S.C. (2013). Enhanced Deep Blue aerosol retrieval algorithm: The second generation. *J. Geophys. Res.* 118: 9296–9315.
- Johnson, B.T., Christopher, S., Haywood, J.M., Osborne, S.R., McFarlane, S., Hsu, C., Salustro, C. and Kahn, R. (2009). Measurements of aerosol properties from aircraft, satellite and ground-based remote sensing: A case-study from the Dust and Biomass-burning Experiment (DABEX). *Q. J. R. Meteorolog. Soc.* 135: 922–934.
- Leahy, L. V., Anderson, T. L., Eck, T.F. and Bergstrom, R.W. (2007). A synthesis of single scattering albedo of biomass burning aerosol over southern Africa during SAFARI 2000. *Geophys. Res. Lett.* 34: L12814.
- Lee, D., Sud, Y.D., Oreopoulos, L., Kim, K.M., Lau, W.K. and Kang, I.S. (2014). Modeling the influences of aerosols on pre-monsoon circulation and rainfall over Southeast Asia. *Atmos. Chem. Phys.* 14: 6853–6866.
- Lin, N.H., Tsay, S.C., Maring, H.B., Yen, M.C., Sheu, G.R., Wang, S.H., Chi, K.H., Chuang, M.T., OuYang, C.F., Fu, J.S., Reid, J.S., Lee, C.T., Wang, L.C., Wang, J.L., Hsu, C.N., Sayer, A.M., Holben, B.N., Chu, Y.C., Nguyen, X.A., Sopajaree, K., Chen, S.J., Cheng, M.T., Tsuang, B.J., Tsai, C.J., Peng, C.M., Schnell, R.C., Conway, T., Chang, C.T., Lin, K.S., Tsai, Y.I., Lee, W.J., Chang, S.C., Liu, J.J., Chiang, W.L., Huang, S.J., Lin, T.H. and Liu, G.R. (2013). An overview of regional experiments on biomass burning aerosols and related pollutants in Southeast Asia: From BASE-ASIA and the Dongsha Experiment to 7-SEAS. *Atmos. Environ.* 78: 1–19.
- Lin, N.H., Sayer, A.M., Wang, S.H., Loftus, A.M., Hsiao, T.C., Sheu, G.R., Hsu, N.C., Tsay, S.C. and Chantara, S. (2014). Interactions between biomass-burning aerosols and clouds over Southeast Asia: Current status, challenges, and perspectives. *Environ. Pollut.* 195: 292–307.
- Loftus, A.M., Tsay, S.C., Pantina, P., Nguyen, C., Gabriel, P.M., Nguyen, X.A., Sayer, A.M., Tao, W.K. and Matsui, T. (2016). Coupled aerosol-cloud systems over Northern Vietnam during 7-SEAS/BASELINE: A radar and modeling perspective. *Aerosol Air Qual. Res.* 16: 2768–2785.
- Paciorek, C.J. and Liu, Y. (2009). Limitations of remotely sensed aerosol as a spatial proxy for fine particulate matter. *Environ. Health Perspect.* 117: 904–909.
- Pantina, P., Tsay, S.C., Hsiao, T.C., Loftus, A.M., Kuo, F., Ou-Yang, C.F., Sayer, A.M., Wang, S.H., Lin, N.H., Hsu, N.C., Janjai, S., Chantara, S. and Nguyen, A.X. (2016). COMMIT in 7-SEAS/BASELINE: Operation of and observations from a novel, mobile laboratory for measuring in-situ properties of aerosols and gases. *Aerosol Air Qual. Res.* 16: 2728–2741.
- Pope, C.A., III (2000). Epidemiology of fine particulate air pollution and human health: biologic mechanisms and who's at risk? *Environ. Health Perspect.* 108: 713–723.
- Reid, J.S., Eck, T.F., Christopher, S.A., Koppmann, R., Dubovik, O., Eleuterio, D.P., Holben, B.N., Reid, E.A. and Zhang, J. (2005). A review of biomass burning emissions part III: intensive optical properties of biomass burning particles. *Atmos. Chem. Phys.* 5: 827–849.
- Reid, J.S., Hyer, E.J., Johnson, R.S., Holben, B.N., Yokelson, R.J., Zhang, J., Campbell, J.R., Christopher, S.A., Di Girolamo, L., Giglio, L., Holz, R.E., Kearney, C., Miettinen, J., Reid, E.A., Turk, F.J., Wang, J., Xian, P., Zhao, G., Balasubramanian, R., Chew, B.N., Janjai, S., Lagrosas, N., Lestari, P., Lin, N.H., Mahmud, M., Nguyen, A.X., Norris, B., Oanh, N.T.K., Oo, M., Salinas, S.V., Welton, E.J. and Liew, S.C. (2013). Observing and understanding the Southeast Asian aerosol system by remote sensing: An initial review and analysis for the Seven Southeast Asian Studies (7SEAS) program. *Atmos. Res.* 122: 403–468.
- Rienecker, M.M., Suarez, M.J., Gelaro, R., Todling, R., Bacmeister, J., Liu, E., Bosilovich, M.G., Schubert, S.D., Takacs, L., Kim, G.K., Bloom, S., Chen, J., Collins, D., Conaty, A., da Silva, A., Gu, W., Joiner, J., Koster, R.D., Lucchesi, R., Molod, A., Owens, T., Pawson, S., Pegion, P., Redder, C.R., Reichle, R., Robertson, F.R., Ruddick, A.G., Sienkiewicz, M. and Woollen, J. (2011). MERRA: NASA's modern-era retrospective analysis for research and applications. *J. Clim.* 24: 3624–3648.
- Sayer, A.M., Hsu, N.C., Bettenhausen, C. and Jeong, M.J. (2013). Validation and uncertainty estimates for MODIS Collection 6 “Deep Blue” aerosol data. *J. Geophys. Res.* 118: 7864–7872.
- Sayer, A.M., Hsu, N.C., Eck, T.F., Smirnov, A. and Holben, B.N. (2014a). AERONET-based models of smoke-dominated aerosol near source regions and transported over oceans, and implications for satellite retrievals of aerosol optical depth. *Atmos. Chem. Phys.* 14: 11493–11523.
- Sayer, A.M., Munchak, L.A., Hsu, N.C., Levy, R.C., Bettenhausen, C. and Jeong, M.J. (2014b). MODIS Collection 6 aerosol products: Comparison between Aqua's e-Deep Blue, Dark Target, and “merged” data sets, and usage recommendations. *J. Geophys. Res.* 119: 13965–13989.
- Sayer, A.M., Hsu, N.C., Bettenhausen, C., Jeong, M.J. and Meister, G. (2015). Effect of MODIS Terra radiometric calibration improvements on Collection 6 Deep Blue aerosol products: Validation and Terra/Aqua consistency. *J. Geophys. Res.* 120: 12157–12174.
- Schafer, J.S., Eck, T.F., Holben, B.N., Thornhill, K.L., Anderson, B.E., Sinyuk, A., Giles, D.M., Winstead, E.L., Ziemba, L.D., Beyersdorf, A.J., Kenny, P.R., Smirnov, A. and Slutsker, I. (2014). Intercomparison of aerosol single-scattering albedo derived from AERONET surface radiometers and LARGE in situ aircraft profiles during the 2011 DRAGON-MD and DISCOVER-AQ experiments. *J. Geophys. Res.* 119: 7439–7452.
- Smirnov, A., Holben, B.N., Eck, T.F., Dubovik, O. and Slutsker, I. (2000). Cloud screening and quality control algorithms for the AERONET database. *Remote Sens. Environ.* 73: 337–349.
- Tipayarom, D. and Oanh, N.T.K. (2007). Effects from open rice straw burning emission on air quality in the Bangkok metropolitan region. *ScienceAsia* 33: 339–345.

- Tsay, S.C., Hsu, N.C., Lau, W.K.M., Li, C., Gabriel, P.M., Ji, Q., Holben, B.N., Judd Welton, E., Nguyen, A.X., Janjai, S., Lin, N.H., Reid, J.S., Boonjawat, J., Howell, S.G., Huebert, B.J., Fu, J.S., Hansell, R.A., Sayer, A.M., Gautam, R., Wang, S.H., Goodloe, C.S., Miko, L.R., Shu, P.K., Loftus, A.M., Huang, J., Kim, J.Y., Jeong, M.J. and Pantina, P. (2013). From BASE-ASIA toward 7-SEAS: A satellite-surface perspective of boreal spring biomass-burning aerosols and clouds in Southeast Asia. *Atmos. Environ.* 78: 20–34.
- Tsay, S.C., Maring, H.B., Lin, N.H., Buntoung, S., Chantara, S., Chuang, H.C., Gabriel, P.M., Goodloe, C.S., Holben, B.N., Hsiao, T.C., Hsu, N.C., Janjai, S., Lau, W.K.M., Lee, C.T., Lee, J., Loftus, A.M., Nguyen, A.X., Nguyen, C.M., Pani, S.K., Pantina, P., Sayer, A.M., Tao, W.K., Wang, S.H., Welton, E.J., Wiriya, W. and Yen, M.C. (2016). Satellite-surface perspectives of air quality and aerosol-cloud effects on the environment: An overview of 7-SEAS/BASELINe. *Aerosol Air Qual. Res.* 16: 2581–2602.
- van der Werf, G.R., Randerson, J.T., Giglio, L., Collatz, G.J., Mu, M., Kasibhatla, P.S., Morton, D.C., DeFries, R.S., Jin, Y. and van Leeuwen, T.T. (2010). Global fire emissions and the contribution of deforestation, savanna, forest, agricultural, and peat fires (1997–2009). *Atmos. Chem. Phys.* 10: 11707–11735.
- van Donkelaar, A., Martin, R.V., Brauer, M., Kahn, R., Levy, R., Verduzco, C. and Villeneuve, P.J. (2010). Global estimates of ambient fine particulate matter concentrations from satellite-based aerosol optical depth: development and application. *Environ. Health Perspect.* 118: 847–855.
- Wang, S.H., Welton, E.J., Holben, B.N., Tsay, S.C., Lin, N.H., Giles, D., Stewart, S.A., Janjai, S., Nguyen, X.A., Hsiao, T.C., Chen, W.N., Lin, T.H., Buntoung, S., Chantata, S. and Wiriya, W. (2015). Vertical Distribution and Columnar Optical Properties of Springtime Biomass-Burning Aerosols over Northern Indochina during 2014 7-SEAS Campaign. *Aerosol Air Qual. Res.* 15: 2037–2050.
- Xu, X., Wang, J., Zeng, J., Spurr, R., Liu, X., Dubovik, O., Li, L., Li, Z., Mishchenko, M.I., Siniuk, A. and Holben, B.N. (2015). Retrieval of aerosol microphysical properties from AERONET photo-polarimetric measurements. 2: A new research algorithm and case demonstration. *J. Geophys. Res.* 120: 7079–7098.

Received for review, August 14, 2015

Revised, October 30, 2015

Accepted, November 25, 2015